Polarization effects in light-tunable Fano resonance in metal-dielectric multilayer structures

Hayashi, S.
Nesterenko, D. V.
Rahmouni, A.
Sekkat, Z.

(Citation)
Physical Review B,95(16):165402-165402

(Issue Date)
2017-04-04

(Resource Type)
journal article

(Version)
Version of Record

Polarization effects in light-tunable Fano resonance in metal-dielectric multilayer structures

S. Hayashi,[1,2,*] D. V. Nesterenko,[1] A. Rahmouni,[1] and Z. Sekkat[1,3,4]

[1]*Optics and Photonics Center, Moroccan Foundation for Science, Innovation and Research (MAScIR), Rabat 10100, Morocco*

[2]*Graduate School of Engineering, Kobe University, Kobe 657-8501, Japan*

[3]*Graduate School of Engineering, Osaka University, Suita 565-0871, Japan*

[4]*Faculty of Sciences, University Mohamed V, Rabat 10010, Morocco*

(Received 17 December 2016; published 4 April 2017)

A planar metal-dielectric multilayer structure containing a waveguide layer doped with azo-dye molecules exhibits a sharp Fano resonance that can be shifted by pump light irradiation owing to a photoinduced change of the refractive index of the waveguide layer by photoisomerization of the azo-dye molecules. Azo-dye-containing materials are polarization sensitive and the photoinduced shift of the Fano resonance is expected to depend on the pump polarization. Previous pump-probe attenuated-total-reflection measurements performed with a normal incidence of pump light exhibited intriguingly no dependence on the pump polarization. In this work, we extend our measurements to an oblique incidence, to optimize the overlap between the pump and probe polarizations, and we demonstrate a strong dependence on the pump polarization. To analyze the experimental results for both the normal and oblique pump conditions, we introduce phenomenological equations, based on the angular hole burning model of the photoisomerization of the azo-dye molecules. The equations allow us to describe the dependence of the refractive index changes in the waveguide layer on the pump angle and polarization. Using the equations, we could obtain good theoretical fits to the experimental data. The results of fitting suggest that the overlap between the pump and probe polarizations plays an important role in determining the amount of the photoinduced shift of the Fano resonance.

DOI: 10.1103/PhysRevB.95.165402

I. INTRODUCTION

Fano resonances characterized by asymmetric line shapes were initially found in atomic spectra [1], and it was Fano who gave a quantum mechanical interpretation as due to the interference of a discrete quantum level with a continuum state [2–4]. The Fano resonances are now known to be omnipresent in a variety of physical systems. Among others, the Fano resonances appearing in the optical response of plasmonic nanostructures and metamaterials attracted much attention in the past decade and have been studied extensively both theoretically and experimentally [4–8]. Metallic nanowire arrays [9], clusters of nanoparticles [10–14], disk/ring nanocavities [15–17], and metal-insulator-metal waveguides coupled to resonators [18] are just a few examples of plasmonic nanostructures that exhibit the Fano resonance. The appearance of the Fano resonances in these nanostructures is commonly attributed to the interaction between a dark electromagnetic (EM) mode with a sharp resonance and a bright EM mode with a broad resonance.

High-Q Fano resonances achieved in these structures are very promising for realizing novel photonic devices with high performances, such as optical sensors and switches [5,6,8]. One of the most important issues in this direction is the tuning of the Fano resonance, not only by the structural parameters but also by applying external perturbations such as the mechanical stress, electric and magnetic fields, and light [8]. Cui *et al.* [19] demonstrated mechanical tuning of Fano resonances supported by a gold heptamer structure embedded in a flexible membrane. Integrating single-layer graphene with plasmonic Fano-resonant metasurfaces, Shvets *et al.* [20,21] succeeded in modulating mid-IR Fano resonances using electrostatic gating. Electric-field modulation of the Fano resonance was also demonstrated for gold nanowire gratings [22] and silicon nanohole arrays [23] integrated with liquid crystals. The Fano resonances tunable by the angle of incidence of exciting light have been demonstrated for a Si nanostripe [24], arrays of tilted aluminum nanowires [25], and Ni nanodisk arrays on a Co film [26]. In spite of the efforts devoted so far, the dynamical tuning of the Fano resonance still remains a challenging task.

In our previous studies [27–30], we have demonstrated theoretically and experimentally the feasibility of generating high-Q Fano resonances in planar metal-dielectric multilayer structures. The structures proposed can be regarded as a combination of a metal-dielectric interface that supports a surface plasmon polariton (SPP) mode and a stack of three dielectric layers that supports a planar waveguide (PWG) mode. The structures are so simple that they can be prepared without nanofabrication techniques. Due to the interaction between the SPP mode with a broad resonance and the PWG mode with a sharp resonance, a Kretschmann configuration consisting of the multilayer structure attached to a glass prism exhibits a sharp Fano line shape in its attenuated total reflection (ATR) spectrum [27,28]. The generation of the sharp Fano line shapes was demonstrated experimentally using multilayer structures composed of an Ag layer, a fluoropolymer Cytop layer, and a poly(methyl methacrylate) (PMMA) layer [29]. Our results of numerical calculations also demonstrate that the structures can lead to extremely high sensing sensitivities and electric field enhancements, when the structural parameters are appropriately chosen [30].

The PMMA layer in our experimental structure acts as a waveguide. Very recently, we reported experimental evidence of light-tunable Fano resonances using the PMMA waveguide layer doped with disperse red 1 (DR1) molecules [31]. The

*s.hayashi@dragon.kobe-u.ac.jp

DR1 molecules are one of the derivatives of azobenzene molecules that undergo the *tras-cis* transformation under optical pumping (photoisomerization) [32–38]. From pump-probe ATR measurements, we demonstrated that the Fano resonance is shifted under pump irradiation and the amount of the shift increases with increasing the pump intensity. In these experiments, the pump light was incident normal to the sample surface and no dependence on the pump polarization was observed. These results are somehow surprising, since the DR1 chromophores are strongly polarization sensitive [39]. The photoinduced shift of the Fano resonance is attributed to the change in the refractive index of the DR1-doped PMMA waveguide layer caused by the photoisomerization.

In the present work, we extend our pump-probe ATR measurements to an oblique incidence of the pump light; an irradiation geometry that allows for an optimized overlap of the pump polarization with that of the probe light at the Fano resonance and consequently, allows for the observation of polarization effects on the phototuning of the Fano resonance. To analyze the results for both the normal and oblique incidence in a coherent way, we apply the angular hole burning (AHB) model [32,33,37], which has commonly been used to describe the changes in linear and nonlinear optical properties of DR1-doped PMMA films under optical pumping (vide infra). Modifying slightly the existing AHB formulation, we derive phenomenological equations that can describe the dependence of the refractive index change on the pump angle and polarization. We show that the equations allow us to obtain good theoretical fits to experimental data. The results of fitting enable us to gain a detailed insight into the mechanism of phototuning of the Fano resonance.

II. EXPERIMENTAL PROCEDURES

The sample and the optical setup used in the present studies are the same as those described in our previous paper [31]. As schematically shown in Fig. 1(a), an Ag layer, a fluoropolymer Cytop layer, and a DR1-doped PMMA layer were successively deposited onto a cleaned SF10 glass substrate. The Ag layer was deposited by a vacuum evaporation technique and the Cytop and DR1-doped PMMA layers were deposited by a spin coating technique. The concentration of DR1 in PMMA was ∼5 wt%. To perform pump-probe ATR measurements in a Kretschmann configuration, the multilayer stack was pasted onto a bottom surface of a 60° prism made of SF11 glass with the aid of index matching fluid.

The optical setup for the pump-probe ATR measurements is schematically shown in Figs. 1(b) and 1(c). The prism with the sample was mounted on a computer-controlled rotating stage. A p-polarized light beam from a He-Ne laser with a wavelength of 632.8 nm, used as probe light, was incident on the sample through the prism, and the intensity of the reflected light beam was measured as a function of the angle of incidence θ_{in} by rotating the stage. For optical pumping of the DR1-doped PMMA layer, a laser beam from a semiconductor laser with a wavelength of 488.0 nm was directed to the sample surface from the air side. In the present optical setup, when the sample stage is rotated to change θ_{in}, the angle of incidence for the pump beam θ_{pump} also changes. Therefore, the pump beam was so aligned to make a desired angle when the probe

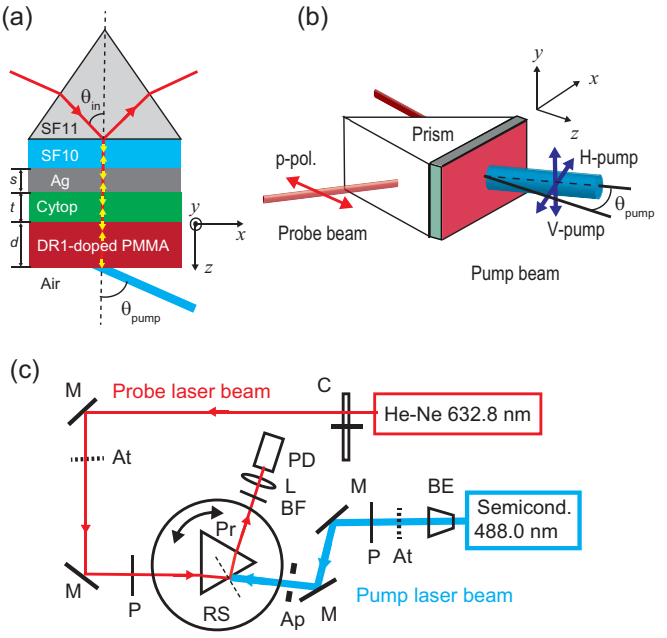

FIG. 1. Sample and optical setup. (a) Multilayer sample prepared on a SF10 glass substrate attached to a SF11 glass prism (Kretschmann configuration). Thicknesses of Ag, Cytop, and DR1-doped PMMA layers determined in our previous work [31] are $s = 45.5$ nm, $t = 524$ nm, and $d = 720$ nm, respectively. Probe light is incident on the sample thorough the prism, and reflected light exiting through the prism after multiple reflection inside the multilayer sample (indicated by arrows) is monitored. (b) Pump and probe beams and directions of their polarization. (c) Setup of pump-probe ATR measurements. Optical elements used are: chopper (C), mirror (M), attenuator (At), polarizer (P), rotation stage (RS), prism (Pr), band-pass filter (BF), lens (L), photodiode (PD), aperture (Ap), and beam expander (BE).

beam scans a narrow angle region of the Fano resonance under the dark condition. Since the width of the Fano resonance in our ATR spectra is of the order of 0.1 deg (internal angle inside the prism), the variation in θ_{pump} around the Fano resonance is of the same order of magnitude (angle in air). To ensure the overlap of the pump beam with the probe beam of ∼2 mm in diameter, the pump beam from the diode laser was first expanded by a beam expander to obtain a beam of ∼10 mm in diameter, and its central part of ∼7 mm in diameter was selected by an aperture and finally directed to the sample surface [see Fig. 1(c)]. The optical pumping was performed with different powers of the pump beam. The pump power density was estimated from the power measured in front of the sample and the cross-sectional area of the pump beam.

As shown in Fig. 1(b), the polarization of the pump beam was set either in the vertical or horizontal direction, referred to as V-pump and H-pump, respectively. In our previous paper, we reported the experimental results obtained with the probe beam directed normal to the sample surface ($\theta_{pump} = 0$), where no appreciable dependence of the shift of the Fano resonance on the pump polarization was observed. In the present paper, we present results obtained under an oblique incidence of the pump beam with $\theta_{pump} = 60$ deg, and demonstrate a strong dependence on the pump polarization. Hereafter, we

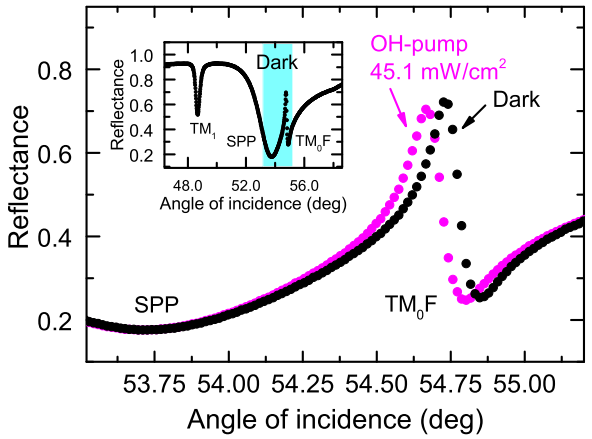

FIG. 2. Comparison between a dark spectrum with a spectrum obtained under OH-pump irradiation with a power density of 45.1 mW/cm^2. The inset shows the dark spectrum in a wider angle range.

call the normal V-pump, normal H-pump, oblique V-pump, and oblique H-pump conditions as NV-, NH-, OV- and OH-pump conditions, respectively. To facilitate the discussion and analysis of the data, we use a Cartesian coordinate system attached to the sample-prism system as shown in Figs. 1(a) and 1(b). The z axis is taken to be normal to the sample surface and the x-y plane is parallel to the interfaces of the multilayer sample. The planes of incidence for the probe and pump beams are on the x-z plane. The horizontal plane in the laboratory system is parallel to the x-z plane and the vertical direction is parallel to the y axis.

III. RESULTS AND DISCUSSION

A. Experimental results

In Fig. 2, an ATR spectrum around the Fano resonance obtained under the OH-pump condition with a power density of 45.1 mW/cm^2 is compared with a spectrum obtained without pump irradiation (dark spectrum). The inset of the figure shows the dark spectrum in a wider angle range. The thicknesses and the dielectric constants of the layers of the present sample determined previously are $s = 45.5$ nm and $\varepsilon_{\mathrm{Ag}} = -16.6 + i2.34$ for the Ag layer, $t = 524$ nm and $\varepsilon_{\mathrm{Cytop}} = 1.83 + i8.11 \times 10^{-3}$ for the Cytop layer, and $d = 720$ nm and $\varepsilon_{\mathrm{PMMA}} = 2.23 + i2.99 \times 10^{-4}$ for the PMMA layer, respectively [31]. As is clear from the inset, the multilayer sample exhibits a sharp Fano resonance (denoted as TM_0F) at the high-angle side of a dip corresponding to the excitation of the SPP mode at the Ag/Cytop interface. The Fano resonance is a consequence of the interference between the SPP mode and the TM_0 PWG mode supported by the DR1-doped PMMA layer. The sample exhibits also a dip at an angle lower than the SPP dip. This dip is due to the excitation of the TM_1 PWG mode. A remarkable feature seen in Fig. 2 is the shift of the Fano resonance to a lower angle under pump irradiation; the SPP dip stays at the same angle under pump irradiation. We note that the photoinduced change in the Fano resonance seen in Fig. 2 is very similar to that previously reported (Fig. 2(b) in Ref. [31]) for the NV-pump condition.

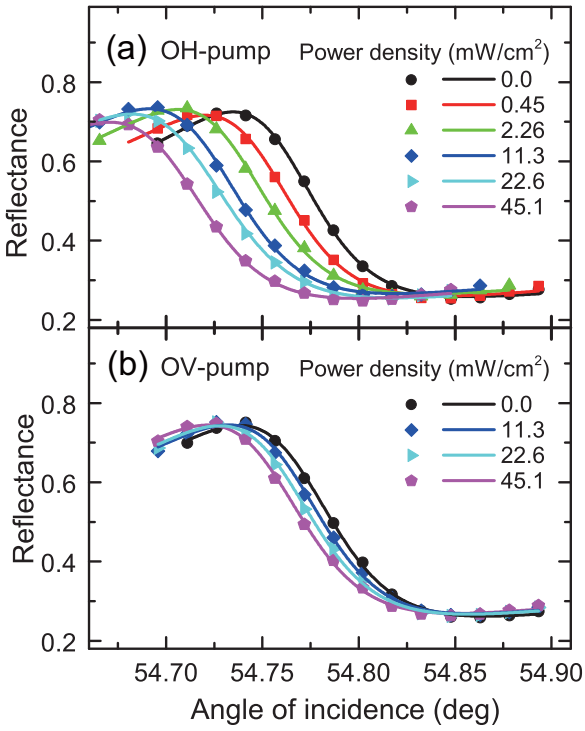

FIG. 3. Results of systematic measurements of the shift of the Fano resonance under (a) OH-pump condition and (b) OV-pump condition. Experimental results are presented by dots and results of Fano fitting are presented by solid curves.

However, a close comparison reveals that the amount of the shift presently observed under the OH pump is considerably larger than the previous one observed under the NV pump, although the pump power density used is the same.

Results of systematic measurements performed under the OH- and OV-pump conditions by varying the pump power density are presented in Figs. 3(a) and 3(b), respectively. We see clearly that for a given power density the shift of the Fano resonance is much larger for the OH pump than for the OV pump. To determine the Fano resonance angles under pump irradiation, the experimental Fano line shapes were fitted to a modified Fano line shape function introduced in our previous paper [31]. The original Fano line shape function describes the line shape as a function of the energy or frequency [2–5]. We rewrote the original function as a function of the angle of incidence and introduced a nonzero minimum value of the reflectance and a scale factor (Eq. (1) in Ref. [31]). The solid curves presented in Figs. 3(a) and 3(b) are the fit curves obtained by the modified Fano function.

From the resonance angles determined from the Fano fits, we define the shift of the resonance as $\Delta\theta = \theta_{\mathrm{irrad}} - \theta_{\mathrm{dark}}$, where θ_{irrad} and θ_{dark} are the resonance angles obtained with and without pump irradiation. In Fig. 4, the absolute value of the shift $|\Delta\theta|$ is plotted as a function of the pump power density for both the OV- and OH-pump conditions together with our previous results obtained under the NV- and NH-pump conditions (Fig. 3 in Ref. [31]). The vertical bar in the figure indicates the precision of the present angular measurements (internal angle inside the prism). The figure demonstrates that the shift increases rapidly in the low power density region

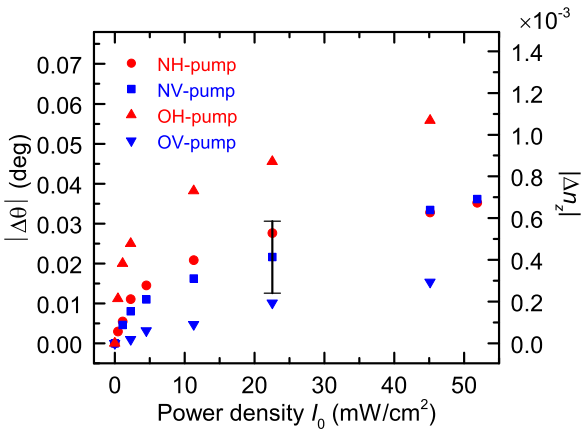

FIG. 4. Shift of the Fano resonance angle plotted as a function of the pump power density obtained for different pump conditions. Right vertical axis represents the change in the refractive index of the DR1-doped waveguide layer converted from the left vertical axis.

and tends to saturate in the high power density region. In case of the normal incidence of the pump beam, there is no discernible difference between the NV- and NH-pump results that exceeds the present angular precision. In contrast, the shift observed under oblique incidence depends strongly on the pump polarization. Figure 4 demonstrates that the OH pump leads to the largest shifts, while the OV pump leads to the smallest shifts.

As discussed in detail in our previous paper [31], the photoinduced shift of the Fano resonance in the present sample is caused by the decrease in the refractive index of the DR1-doped PMMA waveguide layer resulting from the *trans-cis* transformation (photoisomerization) of the DR-1 molecules. To estimate the refractive index change that produces the observed shift, we performed EM calculations of the ATR spectra assuming anisotropic refractive indices n_x, n_y, and n_z for the waveguide layer. The results of calculations indicated that the shift is determined mainly by the refractive index change Δn_z and can be described as $\Delta\theta = S_\theta \Delta n_z$, with a proportionality constant $S_\theta = -52.27$ degRIU^{-1}. This relation allows us to convert $|\Delta\theta|$ to $|\Delta n_z|$ at the probe wavelength. The right vertical axis of Fig. 4 is scaled by $|\Delta n_z|$ converted from $|\Delta\theta|$ of the left vertical axis. We see that $|\Delta n_z|$ values falls in the range of less than $\sim 1.0 \times 10^{-4}$ and those for the OH-pump condition are appreciably larger than those obtained under the NV- and NH-pump conditions.

B. Analysis of photoinduced shifts based on AHB model

To discuss the changes in linear and nonlinear optical properties of DR1-doped polymer films caused by optical pumping, the AHB model has been used widely [32,33,36,40]. In this paper, we use the AHB model to derive analytical expressions for Δn_z, of the photoselectively induced change in the out-of-plane refractive index of the photosensitive layer in the Fano structure, as a function of light polarization, photoisomerization parameters, and irradiation intensity for both the normal and oblique irradiation geometries. First we summarize the existing AHB formulation and then slightly modify it to obtain equations applicable to the present data.

Let us consider a system of DR-1 molecules embedded in a uniform matrix. We can assume that the photoinduced anisotropic change in the refractive index of this composite material is governed by the photoselective isomerization and the photoorientation of the *trans* azo-dye molecules, and the contribution of the *cis* isomer to reorientation is negligible, because it is nearly isotropic; e.g., the molecular polarizability tensor is isotropic. The *trans* molecules are elongated and are considered to be one dimensional and their transition dipole moments can be assumed to have only one component along the long molecular axis. Prior to pump irradiation, the *trans* molecules are assumed to be oriented randomly. Under pump irradiation, the photoisomerization takes place, and when the pump light is polarized linearly, the probability of the *trans-cis* transformation is proportional to $\cos^2\theta_p$, where θ_p is the angle between the molecular axis and the direction of the pump electric field. Since the probability of the transformation is higher for the *trans* molecules oriented closer to the direction of pump electric field, a large depletion of the *trans* molecules oriented in the direction of the polarization of pump light occurs, and a hole is burnt in the angular distribution of the *trans* molecules. The AHB model predicts a larger decrease in the refractive index in the parallel versus perpendicular directions.

Within the framework of the AHB model, the density of the *trans* molecules, oriented in the solid angle $d\Omega$ around a direction Ω specified by angular coordinates as $\Omega = (\theta,\varphi)$, is given by [32,33,40]

$$N_t(\Omega) = \frac{N}{4\pi}(1 + A I_p \cos^2\theta_p)^{-1}, \tag{1}$$

where I_p is the pump intensity (flux of photons) and N is the initial density of randomly oriented *trans* molecules. A is a constant expressed as

$$A = \frac{\sigma_t \Phi_{tc}}{\gamma_{ct}}, \tag{2}$$

where σ_t is the cross section of the molecules for the pump photons, Φ_{tc} is the quantum yield of *trans* to *cis* transformation, and γ_{ct} is the rate of thermal relaxation from the *cis* to *trans* state. Equation (1) indicates that the density of the *trans* molecules decreases through the $\cos^2\theta_p$ term.

When the refractive index of the composite material is monitored by linearly polarized light, the contribution of the *trans* molecules to the refractive index can be written as

$$n_t(I_p) = \alpha_t \int N_t(\Omega)\cos^2\theta_{pr}\, d\Omega, \tag{3}$$

where α_t is the polarizability of a *trans* molecule along the molecular axis and θ_{pr} is the angle between the molecular axis and the probe light electric field. Calculating the change in the refractive index probed by light with the electric field parallel to that of the pump light, one obtains

$$\Delta n_{//} = \alpha_t N\{F_{//}(\zeta) - \tfrac{1}{3}\}, \tag{4}$$

with $\zeta = A I_p$ and

$$F_{//}(\zeta) = \frac{1}{\zeta}\left(1 - \frac{\arctan\sqrt{\zeta}}{\sqrt{\zeta}}\right). \tag{5}$$

In case of the probe electric field perpendicular to that of the pump electric field, one obtains

$$\Delta n_\perp = \alpha_t N\{F_\perp(\zeta) - \tfrac{1}{3}\}, \quad (6)$$

with

$$F_\perp(\zeta) = \frac{1}{2\zeta}\left\{(1+\zeta)\frac{\arctan\sqrt{\zeta}}{\sqrt{\zeta}} - 1\right\}. \quad (7)$$

The pump intensity I_p in Eq. (1) represents the intensity of pump light at the position where the molecules are placed. In our experiments, the pump intensity I_0, which is equivalent to the power density, is estimated in air (outside the sample). Therefore, to apply the above AHB model to analyze our experimental results, it is necessary to find a relation between I_0 in air and I_p inside the DR1-doped waveguide layer. In principle, EM theories allow us to calculate the distributions of the electric fields and light intensities in a multilayer structure generated by incident light, provided that the thicknesses and the optical constants of the layers constituting the structure are known. However, in a structure containing DR1 molecules doped in one of the layers, calculations become very much complex due to two factors. One of them is the anisotropic change in the optical constant of the layer at the pump wavelength caused by photoisomerization of the DR1 molecules. In fact, the decrease in the absorbance of DR1-doped PMMA films at the pump wavelength has been studied carefully and its dichroic behavior has been clearly demonstrated [32,36,37]. The other factor is the nonuniform distribution of the electric field inside the film; the amplitude of electric field depends on the position z in the film. This means that the pump intensity depends on the position z, resulting in position-dependent photoisomerization. Therefore, the changes in the optical constant caused by the photoisomerization are position dependent. The spatial variation of the optical constant in turn influences the electric field distribution. To fully describe the optical processes associated with the photoisomerization, the interplay between the nonuniform optical constant and the nonuniform field distribution has to be taken into account in a self-consistent way. Such EM calculations are highly involved. Furthermore, results of photoisomerization experiments on the optical constant of the DR1-doped PMMA film were reported only for the normal pumping [36,37] and those for the oblique pumping necessary for the present analyses are not available. Since rigorous EM calculations are not tractable at present, we introduce here a simple manner to relate I_0 to I_p as explained below.

We do not incorporate explicitly the effects of photoisomerization of the DR1 molecules and introduce a phenomenological approach. We assume an isotropic refractive index at the pump wavelength that is uniform over the waveguide layer. The electric field and intensity of the pump light inside the waveguide layer is also assumed to be uniform. In general, the intensity of light inside a medium is defined as the amount of energy which crosses, in unit time, an element of area perpendicular to the direction of propagation of an electromagnetic plane wave [41]. This quantity is given by the absolute value of the Poynting vector and can be written as

$$S = \frac{cn}{4\pi}|E|^2 = \frac{cn}{4\pi}(|E_x|^2 + |E_y|^2 + |E_z|^2), \quad (8)$$

where c is the speed of light in the vacuum, n is the isotropic refractive index of the medium, and E is the amplitude of the electric field. For our discussion, it is convenient to define partial intensities corresponding to different components of the electric field by

$$I_p^i(\theta_{pump}) = \frac{cn}{4\pi}|E_i|^2, \quad (i = x,y,z). \quad (9)$$

To connect the external pump intensity to the internal partial pump intensities, we introduce phenomenological factors $a_i(\theta_{pump})$ defined as,

$$I_p^i(\theta_{pump}) = a_i(\theta_{pump})I_0, \quad (i = x,y,z). \quad (10)$$

We assume that the factors $a_i(\theta_{pump})$ depend on the pump angle θ_{pump} and pump polarization. In the present simple approach, the effects of the photoisomerization at the pump wavelength are considered to be incorporated implicitly in the phenomenological factors.

We performed our pump-probe ATR measurements under NV-, NH-, OV-, and OH-pump conditions. We now derive equations that describe Δn_z for different pump conditions. Under the NV-pump condition ($\theta_{pump} = 0^\circ$), the electric field of pump light has only the E_y component that generates the E_y component inside the DR1-doped waveguide layer; corresponding partial pump intensity is thus $I_p^y = a_y(0)I_0$. In this case, the pump electric field is perpendicular to the probe direction of the refractive index change (z direction). Therefore, the contribution of the pump light to Δn_z at the probe wavelength is given by $\Delta n_\perp$ [Eq. (6)], when I_p is replaced by $a_y(0)I_0$. Rewriting $Aa_y(0)$ and $\alpha_t N$ simply as $A_\perp^N$ and D, respectively, and putting $\eta = A_\perp^N I_0$ we obtain

$$\Delta n_z^{NV}(I_0) = D\{F_\perp(\eta) - \tfrac{1}{3}\}. \quad (11)$$

The function $F_\perp(\eta)$ is given by Eq. (7). Under the NH-pump condition, the external pump electric field has only the E_x component that generates the E_x component inside the waveguide layer, resulting in a partial intensity $I_p^x = a_x(0)I_0$. Because the planar multilayer structure has a rotational symmetry around the z axis, we can set as $a_x(0) = a_y(0)$, which results in

$$\Delta n_z^{NH}(I_0) = \Delta n_z^{NV}(I_0). \quad (12)$$

This theoretical result is in good agreement with the experimental finding that the NV-pump and NH-pump conditions do not lead to observable differences in the photoinduced shift of the Fano resonance (or in Δn_z).

Under the OV-pump condition, the external pump light has only the E_y component. Repeating the same argument as that for the NV-pump case, we arrive at an expression of $\Delta n_z^{OV}(I_0)$, which is the same as $\Delta n_z^{NV}(I_0)$ [Eq. (11)], when $a_y(0)$ is replaced by $a_y(60)$ for $\theta_{pump} = 60^\circ$. Rewriting $Aa_y(60)$ as $B_\perp^O$ and setting $\xi = B_\perp^O I_0$, we obtain

$$\Delta n_z^{OV}(I_0) = D\{F_\perp(\xi) - \tfrac{1}{3}\}. \quad (13)$$

Under the OH-pump condition, the pump light has E_x and E_z components, and consequently both the E_x and E_z components are induced inside the DR1-doped waveguide layer; corresponding partial intensities are written as $I_p^x = a_x(60)I_0$ and $I_p^z = a_z(60)I_0$. In this case, Δn_z at the probe wavelength

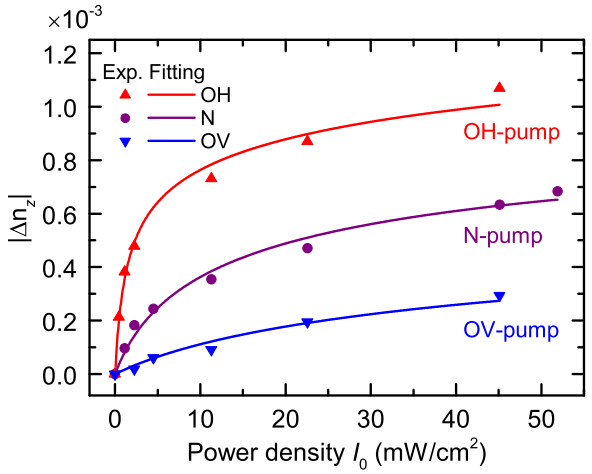

FIG. 5. Refractive index change vs pump power density replotted from Fig. 4 (dots). Solid curves are the theoretical fits to the experimental points obtained by Eqs. (11), (14), and (15).

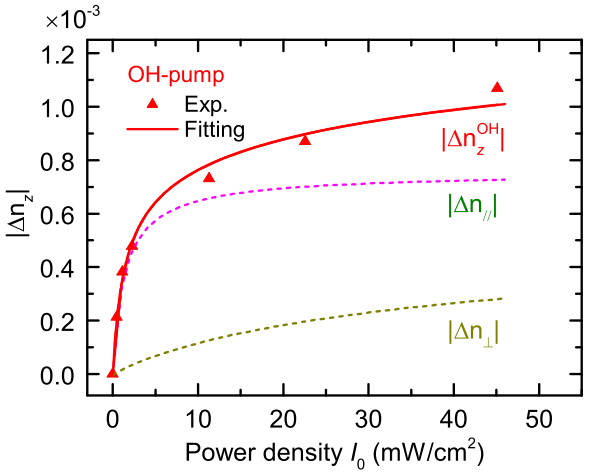

FIG. 6. Separation of the contributions of $\Delta n_{//}$ and $\Delta n_{\perp}$ to the total contribution Δn_z.

is given by a summation of two terms as

$$\Delta n_z^{\mathrm{OH}}(I_0) = \Delta n_{\perp}(a_x(60)I_0) + \Delta n_{//}(a_z(60)I_0). \qquad (14)$$

Rewriting simply $Aa_x(60)$ and $Aa_z(60)$ as $C_{\perp}^{\mathrm{O}}$ and $C_{//}^{\mathrm{O}}$, respectively, we finally obtain

$$\Delta n_z^{\mathrm{OH}}(I_0) = D\left[\left\{F_{\perp}(\rho) - \tfrac{1}{3}\right\} + \left\{F_{//}(\sigma) - \tfrac{1}{3}\right\}\right], \qquad (15)$$

where ρ and σ represent $C_{\perp}^{\mathrm{O}}I_0$ and $C_{//}^{\mathrm{O}}I_0$, respectively.

Here, we examine whether the data of Δn_z can be well described or not by the above expressions of $\Delta n_z^{\mathrm{NV}}(I_0)$, $\Delta n_z^{\mathrm{NH}}(I_0)$, $\Delta n_z^{\mathrm{OV}}(I_0)$, and $\Delta n_z^{\mathrm{OH}}(I_0)$. To facilitate the analysis and discussion, the experimental values of $|\Delta n_z|$ converted from experimental values of $|\Delta\theta|$ are replotted in Fig. 5. Under the NV- and NH-pump conditions, no appreciable dependence on the pump polarization was observed. Therefore, we plot average values of $|\Delta n_z|$ obtained for the V- and H-pump conditions. The resulting data is simply referred to N-pump data.

We performed the fitting of the experimental data to theoretical curves calculated by Eqs. (11), (13) and (15), taking D, $A_{\perp}^{\mathrm{N}}$, $B_{\perp}^{\mathrm{O}}$, $C_{\perp}^{\mathrm{O}}$, and $C_{//}^{\mathrm{O}}$ as fitting parameters. To find the best fit values of the parameters, we used a nonlinear least-square fitting method based on the Levenberg-Marquart algorithm, which is included in the Origin software package. The results of fitting are shown in Fig. 5 by solid curves. The fit curve for the N-pump data was generated by $D = 3.24 \times 10^{-3}$ and $A_{\perp}^{\mathrm{N}} = 0.397(\mathrm{cm}^2/\mathrm{mW})$. The theoretical fit to the OV-pump data was obtained by $D = 2.27 \times 10^{-3}$ and $B_{\perp}^{\mathrm{O}} = 0.103(\mathrm{cm}^2/\mathrm{mW})$, while that to the OH-pump data by $D = 2.27 \times 10^{-3}$, $C_{\perp}^{\mathrm{O}} = 0.108(\mathrm{cm}^2/\mathrm{mW})$, and $C_{//}^{\mathrm{O}} = 1.33(\mathrm{cm}^2/\mathrm{mW})$. We see that the theoretical curves reproduce well the observed dependencies of $|\Delta n_z|$ on I_0 for different pump conditions. In principle, the value of D must be a constant for a given sample, when the concentration of the DR1 molecules is uniform over the sample. However, it was necessary to use different values for the data sets taken with the normal incidence and the oblique incidence. In our experiments, the different data sets were obtained for different points of the same sample. Although the reason why we need different D values is not totally clear at present, a possible reason is the variation of the concentration of the DR1 molecules depending on the sample point.

In Fig. 5, we see that the OV-pump data are smaller than the N-pump data. According to the above results of fitting, this can be attributed partly to the smaller D value for the OV-pump condition and partly to the $B_{\perp}^{\mathrm{O}}$ value smaller than the $A_{\perp}^{\mathrm{N}}$ value. From the derivations given above, it is clear that the smaller $B_{\perp}^{\mathrm{O}}$ value implies a smaller partial intensity $I_{\mathrm{p}}^{y}(60)$ relative to $I_{\mathrm{p}}^{y}(0)$. The decrease in the partial intensity, when the pump beam is inclined from the normal incidence to oblique incidence, is a general behavior predicted from simple EM calculations neglecting the effects of photoisomerization at the pump wavelength.

The OH-pump data in Fig. 5 take values larger than those of the OV-pump and N-pump data. It should be noted that the OH-pump fit function given by Eqs. (14) and (15) contains the contribution of $\Delta n_{//}$ in addition to that of $\Delta n_{\perp}$. To clarify the relative importance of these contributions, they are plotted separately in Fig. 6, together with the total contribution and experimental points. We see that the contribution of $\Delta n_{\perp}$ is almost the same as that for the OV pump, while $\Delta n_{//}$ contributes largely to increase the total values, in particular in the region of low pump power densities. According to the results of fitting, the large contribution of $\Delta n_{//}$ stems from the large $C_{//}^{\mathrm{O}}$ value, which suggests a large partial intensity $I_{\mathrm{p}}^{z}(60)$ relative to $I_{\mathrm{p}}^{y}(0)$.

The large $I_{\mathrm{p}}^{z}(60)$ is not predicted by the EM calculations neglecting the effects of photoisomerization. However, we can explain the relative increase in $I_{\mathrm{p}}^{z}(60)$, at least qualitatively, by taking into account the effects of the photoisomerization on the imaginary part of n_z of the DR1-doped PMMA waveguide layer at the pump wavelength. As demonstrated experimentally and analyzed theoretically in Refs. [37,40], the absorbance of DR1-doped PMMA films at the pump wavelength, which is related directly to the imaginary part of the refractive index of the films, decreases considerably under pump irradiation. The decrease in the absorbance in the direction of the pump polarization (parallel contribution)

is much larger than that in the direction perpendicular to the pump polarization (perpendicular contribution) (see Fig. 1(c) in Ref. [37]). Under the N-pump condition, the pump light has no E_z component and the decrease in the imaginary part of n_z is induced only by the perpendicular field, E_x or E_y. Under the OH-pump condition, the pump light has nonzero E_z fields that induce parallel contribution to n_z in addition to the perpendicular contribution induced by E_x fields. Consequently, the photoisomerization under the OH pump induces a decrease in the imaginary part of n_z much larger than that under the N pump. A smaller imaginary part of n_z in turn induces larger E_z fields and finally generates a larger partial intensity $I_p^z(60)$. Further theoretical considerations that take into account explicitly the effects of photoisomerization on the optical constants at the pump wavelength, as well as the nonuniformity in the EM fields and in the optical constants, may be required to fully explain the present experimental data. Nevertheless, the present phenomenological approach allows us to obtain good fits to the experimental data and suggests the important contribution of $\Delta n_{//}$ to Δn_z under the OH-pump condition, in addition to that of $\Delta n_\perp$. In brief, a large refractive index change observed in the OH-pump geometry is due to the existence of the E_z component of the pump light that overlaps with that of the probe light at the Fano resonance, which is absent in other pump geometries.

IV. CONCLUSION

We have presented and analyzed the results of pump-probe ATR experiments on the Fano resonance in the multilayer structure that contains the DR1-doped PMMA waveguide layer. Due to the *trans-cis* transformation (photoisomerization) of the DR1 molecules, the resonance angle of the Fano line shape is shifted under pump irradiation. When the pump beam is incident normal to the waveguide layer, no appreciable dependence of the shift on the pump polarization is observed. In contrast, the measurements performed with the oblique incidence show a strong dependence of the shift on the pump polarization. With the aid of EM calculations of the ATR spectra, the observed angular shifts were converted to the changes in the refractive index of the waveguide layer. To analyze in a coherent way the different data of refractive index change corresponding to the different pump geometries, we derived phenomenological equations modifying the existing AHB model. We demonstrated that the dependencies of the refractive index change on the pump angle and pump polarization can be well fitted by theoretical curves calculated by the phenomenological equations. Furthermore, the results of fitting allowed us to recognize the importance of the overlap between the pump electric fields and the probe electric fields at the Fano resonance. Experimental and theoretical results presented here open the way to understand the mechanism of photoinduced shift of the Fano resonance and thereby develop photonic devices based on the light-tunable Fano resonance in the multilayer structure.

ACKNOWLEDGMENTS

This work was partially supported by the Moroccan Ministry for Higher Education and Research in the framework of priority research projects (PRP), the Osaka University International Joint Research Promotion Program, and the JSPS KAKENHI (Grant No. 16K04979).

[1] H. Beutler, Z. Phys. A **93**, 177 (1935).
[2] U. Fano, Il Nuovo Cimento **12**, 154 (1935).
[3] U. Fano, Phys. Rev. **124**, 1866 (1961).
[4] A. E. Miroshnichenko, S. Flach, and Y. S. Kivshar, Rev. Mod. Phys. **82**, 2257 (2010).
[5] B. Luk'yanchuk, N. I. Zheludev, S. A. Maier, N. J. Halas, P. Nordlander, H. Giessen, and C. T. Chong, Nat. Mater. **9**, 707 (2010).
[6] N. J. Halas, S. Lal, W.-S. Chang, S. Link, and P. Nordlander, Chem. Rev. **111**, 3913 (2011).
[7] A. B. Khanikaev, C. Wu, and G. Shvets, Nanophotonics **2**, 247 (2013).
[8] M. Rahmani, B. Luk'yanchuk, and M. Hong, Laser Photonics Rev. **7**, 329 (2013).
[9] A. Christ, Y. Ekinci, H. H. Solak, N. A. Gippius, S. G. Tikhodeev, and O. J. F. Martin, Phys. Rev. B **76**, 201405(R) (2007).
[10] J. B. Lassister, H. Sobhani, J. A. Fan, J. Kundu, F. Capasso, P. Nordlander, and N. J. Halas, Nano Lett. **10**, 3184 (2010).
[11] J. B. Lassister, H. Sobhani, M. W. M. W. S. Knight, P. Nordlander, and N. J. Halas, Nano Lett. **12**, 1058 (2011).
[12] S. N. Sheikholeslami, A. Garcia-Extarri, and J. A. Dionne, Nnao Lett. **11**, 3927 (2011).
[13] W.-S. Chang, J. B. Lassister, P. Swanglap, H. Sobhani, S. Khatua, P. Nordlander, N. J. Halas, and S. Link, Nano Lett. **12**, 4977 (2012).
[14] Z.-J. Yang, Q.-Q. Wang, and H.-Q. Lin, Appl. Phys. Lett. **103**, 111115 (2013).
[15] Y. Sonnerfraud, N. Verellen, H. Sobhani, G. A. E. Vandenbosch, V. V. Moshchalkov, P. V. Dorpe, P. Nordlander, and S. A. Maier, ASC Nano **4**, 1664 (2010).
[16] Y. H. Fu, J. B. Zhang, Y. F. Yu, and B. Luk'yanchuk, ACS Nano **6**, 5130 (2012).
[17] J. Li, T. Liu, H. Zheng, J. Dong, E. He, W. Gao, Q. Han, C. Wang, and Y. Wu, Plasmonics **9**, 1439 (2014).
[18] J. Qi, C. Z., J. Chen, Y. Li, W. Qiang, J. Xu, and Q. Sun, Opt. Express **22**, 14688 (2014).
[19] Y. Cui, J. Zhou, V. A. Tamma, and W. Park, ACS Nano **6**, 2385 (2012).
[20] S. H. Mousavi, I. Kholmanov, K. Alici, D. Purtseladze, N. Arju, K. Tatar, D. Y. Fozdar, J. W. Suk, Y. Hao, A. B. Khanikaev, R. Ruoff, and G. Shvets, Nano Lett. **13**, 1111 (2013).
[21] N. Dabidian, I. Kholmanov, A. Khanikaev, K. Tatar, S. Trendafilov, S. H. Mousavi, C. Magnuson, R. S. Ruoff, and G. Shvets, ACS Photonics **2**, 216 (2015).
[22] F. Zhang, X. Hu, C. Wu, H. Yang, and Q. Gong, Appl. Phys. Lett. **105**, 181114 (2014).
[23] W. Zhao, H. Jiang, B. Liu, Y. Jiang, C. Tang, and J. Li, Appl. Phys. Lett. **107**, 171109 (2015).
[24] P. Fan, Z. Yu, S. Fan, and M. L. Brongersma, Nat. Mater. **13**, 471 (2014).

[25] L. Duenmpelmann, D. Casari, A. Lu-Dinh, B. Gallinet, and L. Novotny, ACS Nano **9**, 12383 (2015).
[26] L. Chen, J. Gao, W. Xia, S. Zhang, S. Tang, W. Zhang, D. Li, X. Wu, and Y. Du, Phys. Rev. B **93**, 214411 (2016).
[27] S. Hayashi, D. V. Nesterenko, and Z. Sekkat, Appl. Phys. Express **8**, 022201 (2015).
[28] S. Hayashi, D. V. Nesterenko, and Z. Sekkat, J. Phys. D: Appl. Phys. **48**, 325303 (2015).
[29] S. Hayashi, D. V. Nesterenko, A. Rahmouni, and Z. Sekkat, Appl. Phys. Lett. **108**, 051101 (2016).
[30] D. V. Nesterenko, S. Hayashi, and Z. Sekkat, J. Opt. **18**, 065004 (2016).
[31] S. Hayashi, D. V. Nesterenko, A. Rahmouni, H. Ishitobi, Y. Inouye, and S. Kawata, Sci. Rep. **6**, 33144 (2016).
[32] Z. Sekkat, *Photoreactive Organic Thin Films*, edited by Z. Sekkat and W. Knoll (Academic, New York, 2002).
[33] Z. Sekkat and M. Dumont, Appl. Phys. B **53**, 121 (1991).
[34] M. Dumont, D. Morichère, Z. Sekkat, and Y. Levy, in *SPIE Vol. 1559 Photopolymer Device Physics, Chemistry, and Applications II* (SPIE-The International Society for Optical Engineering, Bellingham, 1991), p. 127.
[35] Z. Sekkat, D. Morichère, M. Dumont, R. Loucif-Saïbi, and J. A. Delaire, J. Appl. Phys. **71**, 1543 (1992).
[36] Z. Sekkat and M. Dumont, Appl. Phys. B **54**, 486 (1992).
[37] Z. Sekkat and M. Dumont, Synth. Met. **54**, 373 (1993).
[38] Z. Sekkat, Appl. Opt. **55**, 259 (2016).
[39] A. Rahmouni, Y. Bougdid, S. Moujdi, D. V. Nesterenko, and Z. Sekkat, J. Phys. Chem. B **120**, 11317 (2016).
[40] M. Dumont and Z. Sekkat, in *SPIE Vol. 1774 Nonconducting Photopolymers and Applications*, edited by R. A. Lessard (SPIE-The International Society for Optical Engineering, Bellingham, 1992), p. 188.
[41] M. Born and E. Wolf, *Principles of optics*, 7th ed. (Cambridge University Press, Cambridge, 1999), pp. 24–25.